Symmetry as a Continuous Feature

H. Zabrodsky S. Peleg D. Avnir*

Institute of Computer Science
The Hebrew University of Jerusalem
91904 Jerusalem, Israel
email: gigi@cs.huji.ac.il

Abstract

Symmetry is treated as a continuous feature and a Continuous Measure of Distance from Symmetry in shapes is defined. The Symmetry Distance (SD) of a shape is defined to be the minimum mean squared distance required to move points of the original shape in order to obtain a symmetrical shape. This general definition of a symmetry measure enables a comparison of the "amount" of symmetry of different shapes and the "amount" of different symmetries of a single shape. This measure is applicable to any type of symmetry in any dimension. The Symmetry Distance gives rise to a method of reconstructing symmetry of occluded shapes. We extend the method to deal with symmetries of noisy and fuzzy data. Finally, we consider grayscale images as 3D shapes, and use the Symmetry Distance to find the orientation of symmetric objects from their images, and to find locally symmetric regions in images.

*Department of Organic Chemistry

1 Introduction

One of the basic features of shapes and objects is symmetry. Symmetry is considered a pre-attentive feature which enhances recognition and reconstruction of shapes and objects [4]. Symmetry is also an important parameter in physical and chemical processes and is an important criterion in medical diagnosis.

a.  b.  c. 

Figure 1: Faces are not perfectly symmetrical.
a) Original image.
b) Right half of original image and its reflection.
c) Left half of original image and its reflection.

However, the exact mathematical definition of symmetry [28, 38] is inadequate to describe and quantify the symmetries found in the natural world nor those found in the visual world (a classic example is that of faces - see Figure 1). Furthermore, even perfectly symmetric objects loose their exact symmetry when projected onto the image plane or the retina due to occlusion, perspective transformations, digitization, etc. Thus, although symmetry is usually considered a binary feature, (i.e. an object is either symmetric or it is not symmetric), we view symmetry as a continuous feature where intermediate values of symmetry denote some intermediate "amount" of symmetry. This concept of continuous symmetry is in accord with our perception of symmetry as can be seen, for example, the shapes shown in Figure 2a.

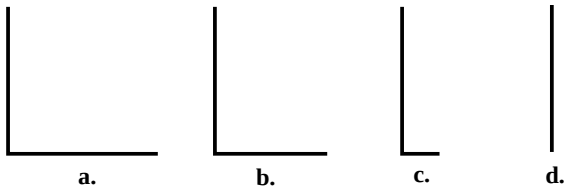

Figure 2: Perceiving continuous symmetry.
a) A shape perceived as perfectly symmetric (the oblique mirror axis passing through the vertex).
b) Shortening one arm, the shape is perceived as "almost" symmetric.
c) Further shortening of the arm, the shape is perceived as having "less" symmetry.
e) When the arm is eliminated the the shape is again perfectly symmetric (with a mirror axis perpendicular to the existing arm).

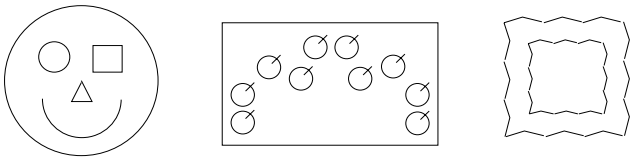

Figure 3: Figures which are more symmetric at low resolution than at high resolution.

Considering symmmetry as a continuous feature, we introduce a "Symmetry Distance" that can measure and quantify all types of symmetries of objects. This measure will enable a comparison of the "amount" of symmetry of different shapes and the "amount" of different symmetries of a single shape.

Once symmetry is considered a continuous feature, it becomes dependent on the resolution by which the scene is viewed. Figure 3 shows examples which are more symmetrical at low resolutions than at high resolutions. Julesz et. al. [22] showed that separation into frequency channels precedes symmetry detection, thus different symmetries can be seen simultaneously in an image. In general, however, the symmetries found at high resolution also exist at low resolution. Studies [26] have shown that human scanning of mirror-symmetric images is concentrated on one mirror-half of the image, implying that the symmetry detection process uses low spatial frequencies for guiding the scanning process. We use a similar approach by combining the Symmetry Distance with a multiresolution scheme to find locally symmetric regions in images.

In Section 1.2 we briefly review some previous studies on symmetry in computer vision. In Section 2 we define the Symmetry Distance and in Section 3 describe a method for evaluting this measure. Following, in Sections 4-6 we describe features of the symmetry distance including its use in dealing with occluded objects and with noisy data. Finally in Section 7 we describe the application of the symmetry distance to finding face orientation and to finding locally symmetric regions in images.

1.1 Definitions of Symmetry

Following are the definitions of symmetry as will be referred to in this paper. For further details and an excellent review see [38].

An n-dimensional object has **mirror-symmetry** if it is invariant under a reflection about a hyperplane of dimension $(n-1)$ passing through the center of mass of the object. Thus a 2D

object is mirror-symmetric if it is invariant under a reflection about a line (called the axis of mirror-symmetry) and a 3D object is mirror-symmetric if it is invariant under a reflection about a plane.

A 2D object has **rotational-symmetry** of order n if it is invariant under rotation of $\frac{2\pi}{n}$ radians about the center of mass of the object.

A 3D object has **rotational-symmetry** of order n if it is invariant under rotation of $\frac{2\pi}{n}$ radians about a line passing through the center of mass of the object (denoted rotational symmetry axis).

Rotational symmetry of order n is denoted $\mathbf{C_n}$**-Symmetry**.

Radial symmetry (referred to in Section 1.2) is the symmetry of a 2D object having both mirror-symmetry and C_n-symmetry (note that such objects have $2n$ axes of mirror-symmetry). Radial symmetry of order n is denoted $\mathbf{D_n}$**-Symmetry**. Circular symmetry (referred to in Section 1.2) is C_∞-symmetry (see Figure 4).

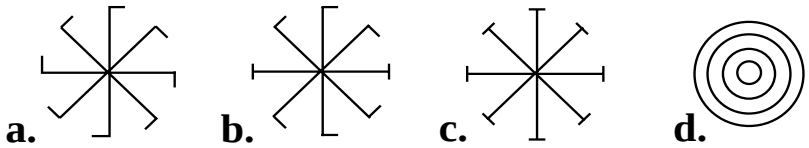

Figure 4: Examples of symmetries: a) C_8-symmetry b) mirror-symmetry c) D_8-symmetry (radial symmetry of order 8). d) circular symmetry (C_∞-symmetry).

1.2 Studies of Symmetry In Computer Vision

As an intrinsic characteristic of objects and shapes, symmetry can be used to describe and recognize objects. True symmetrical shapes can be described on a global scale [20, 25] while most general shape description require local symmetry evaluation [11, 32]. Symmetrical features of images have been exploited for better image compression [24]. Symmetrical descriptions of shapes [9, 11, 15, 21] or detection of symmetrical features of objects [34] can be useful in guiding shape matching, model-based object matching and object recognition [31, 33]. Reconstruction of 3D objects has also been implemented using symmetry as a constraint [36, 14, 29]. More recently, symmetry has been used to discriminate textures [10] and has been used in guiding robot grasping [8].

Transformation of the symmetry detection problem to a pattern matching problem introduces efficient algorithms for detection of mirror and rotational symmetries and location of symmetry axis [3, 19, 1]. These algorithms assume noise free input and detect symmetry, if it exists, on a global scale. Slight perturbation of the input will fail symmetry detection. However, upper bounds on the complexity of symmetry detection with a limited error tolerance has been presented [1]. Local circular (radial) symmetries have been detected and located in images [6, 34]. Mirror and linear symmetries have been detected in images of single objects (global symmetry) and extended to local symmetries [7, 27]. Additional work on skewed symmetry detection was presented [37, 31].

So far, symmetry has been treated as a binary feature: either it exists or it does not exist. However, even when objects in the world are symmetrical, their projection onto a digital image is not necessarily so. Perspective projection, inconsistent lighting, digitization and quantization do not usually preserve exact symmetry. Furthermore, existence of several objects in the scene requires a notion of local symmetries, while occluded symmetries and partial symmetries should also be dealt with.

In an early work, Grünbaum [17] reviews methods of geometrically measuring symmetry of convex sets. Yodogawa [39] has presented an evaluation of symmetry (namely "Symmetropy") in single patterns which uses information theory to evaluate the distribution of symmetries in a pattern. Marola [27] presents a coefficient of mirror-symmetry with respect to a given axis. Global mirror-symmetry of an object (image) is found by roughly estimating the axis location and then fine tuning the location by minimizing the symmetry coefficient. Gilat [16], Hel-Or et.al.[18] and Avnir et.al. [5] present the idea of a *Measure of Chirality* (a measure of deviation from mirror-symmetry). Similar to Marola, Gilat's chirality measure is based on minimizing the volume difference between the object and it's reflection through a varying plane of reflection. Hel-Or et al. present a measure of chirality for 2D objects based on rotational effects of chiral bodies on the surround.

These symmetry detection and evaluation methods are each limited to a certain type of symmetry (mirror or circular symmetry). In this paper we introduce the notion of a *symmetry distance* and present a general continuous measure for evaluating all types of symmetries in any dimension.

2 A Continuous Symmetry Measure - Definition

We define the **Symmetry Distance** (SD) as a quantifier of the minimum effort required to turn a given shape into a symmetric shape. This effort is measured by the mean of the square distances each point is moved from its location in the original shape to its location in the symmetric shape. Note that no a priori symmetric reference shape is assumed.

Denote by Ω the space of all shapes of a given dimension, where each shape P is represented by a sequence of n points $\{P_i\}_{i=0}^{n-1}$. We define a metric d on this space as follows:

$$d : \Omega \times \Omega \rightarrow R$$

$$d(P,Q) = d(\{P_i\},\{Q_i\}) = \frac{1}{n}\sum_{i=0}^{n-1} \|P_i - Q_i\|^2$$

This metric defines a distance function between every two shapes in Ω.

We define the **Symmetry Transform** ST of a shape P, as the symmetric shape closest to P in terms of the metric d.

The **Symmetry Distance (SD)** of a shape P is now defined as the distance between P and it's Symmetry Transform:

$$SD = d(P, ST(P))$$

The SD of a shape $P = \{P_i\}_{i=0}^{n-1}$ is evaluated by finding the symmetry transform $\hat{P}$ of P (Figure5) and computing: $\boxed{\text{SD} = \frac{1}{n}\Sigma_{i=0}^{n-1}\|P_i - \hat{P}_i\|^2}$.

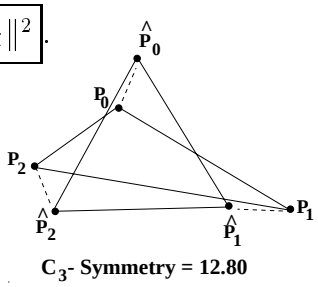

Figure 5: The symmetry transform of $\{P_0, P_1, P_2\}$ is $\{\hat{P}_0, \hat{P}_1, \hat{P}_2\}$. SD = $\frac{1}{3}\Sigma_{i=0}^{2}\|P_i - \hat{P}_i\|^2$

This definition of the Symmetry Distance implicitly implies invariance to rotation and translation. Normalization of the original shape prior to the transformation additionally allows invariance to scale (Figure 6). We normalize by scaling the shape so that the maximum distance between points on the contour and the centroid is a given constant (in this paper all examples are given following normalization to 100). The normalization presents an upper bound of on the mean squared distance moved by points of the shape. Thus the SD value is limited in range, where SD=0 for perfectly symmetric shapes (see Appendix in [43]). The general definition of the Symmetry Distance enables evaluation of a given shape for different

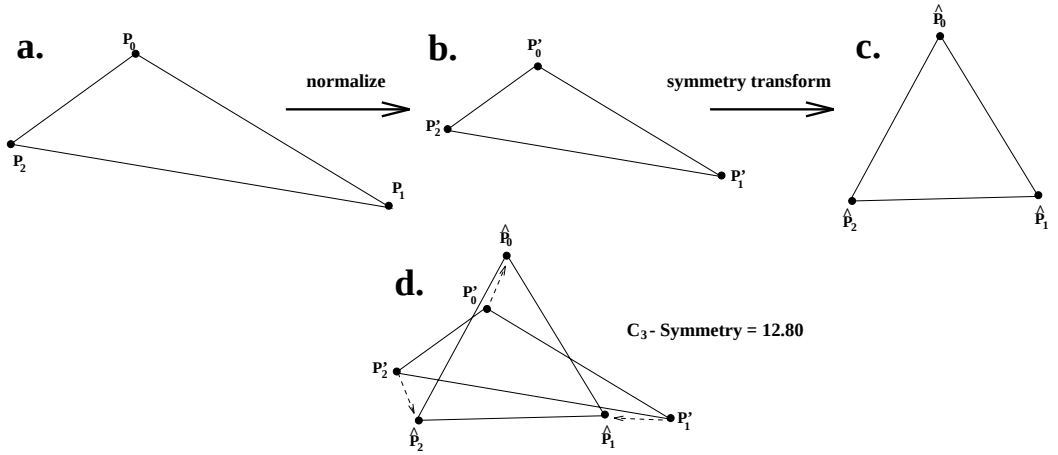

Figure 6: Calculating the Symmetry Distance of a shape:
a) Original shape $\{P_0, P_1, P_2\}$.
b) Normalized shape $\{P_0', P_1', P_2'\}$, such that maximum distance to the center of mass is one.
c) Applying the symmetry transform to obtain a symmetric shape $\{\hat{P}_0, \hat{P}_1, \hat{P}_2\}$.
d) SD $= \frac{1}{3}(\|P_0' - \hat{P}_0\|^2 + \|P_1' - \hat{P}_1\|^2 + \|P_2' - \hat{P}_2\|^2)$
SD values are multiplied by 100 for convenience of handling.

types of symmetries (mirror-symmetries, rotational symmetries etc). Moreover, this generalization allows comparisons between the different symmetry types, and allows expressions such as "a shape is more mirror-symmetric than rotationally-symmetric of order two". An additional feature of the Symmetry Distance is that we obtain the symmetric shape which is 'closest' to the given one, enabling visual evaluation of the SD.

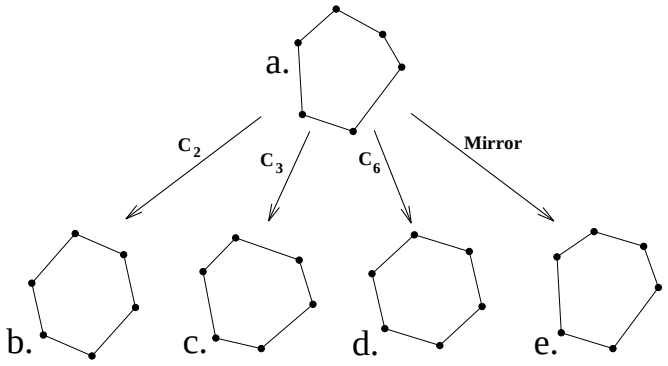

Figure 7: Symmetry Transforms and Symmetry Distances of a 2D polygon.
a) The 2D polygon.
b) Symmetry Transform of (a) with respect to C_2-symmetry (SD = 1.87).
c) Symmetry Transform of (a) with respect to C_3-symmetry (SD = 1.64).
d) Symmetry Transform of (a) with respect to C_6-symmetry (SD = 2.53).
e) Symmetry Transform of (a) with respect to Mirror-symmetry (SD = 0.66).

An example of a 2D polygon and it's symmetry transforms and SD values are shown in Figure 7. Note that shape 7e is the most similar to the original shape 7a and, indeed, its SD

value is the smallest. In the next Section we describe a geometric algorithm for deriving the Symmetry Transform of a shape. In Section 4 we deal with the initial step of representing a shape by a collection of points.

3 Evaluating the Symmetry Transform

In this Section we describe a geometric algorithm for deriving the Symmetry Transform of a shape represented by a sequence of points $\{P_i\}_{i=0}^{n-1}$. In practice we find the Symmetry Transform of the shape with respect to a given point-symmetry group (see Appendix A.1 for a review of algebraic definitions). For simplicity and clarity of explanation, we describe the method by using some examples. Mathematical proofs and derivations can be found in Appendix A.2.

Following is a geometrical algorithm for deriving the symmetry transform of a shape P having n points with respect to rotational symmetry of order n (C_n-symmetry). This method transforms P into a regular n-gon, keeping the centroid in place.

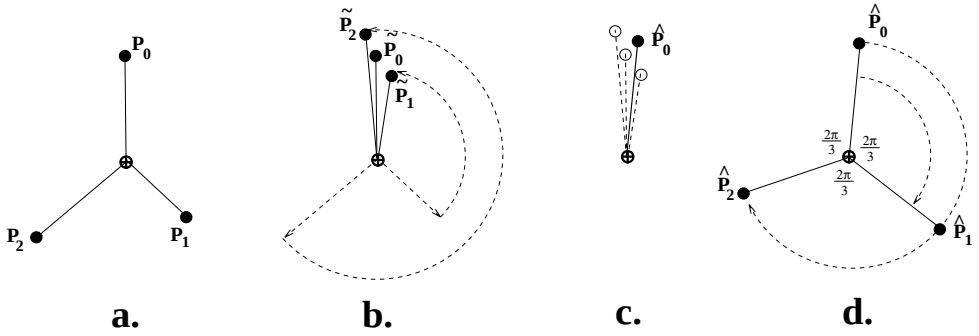

Figure 8: The C_3-symmetry Transform of 3 points.
a) original 3 points $\{P_i\}_{i=0}^{2}$.
b) Fold $\{P_i\}_{i=0}^{2}$ into $\{\tilde{P}_i\}_{i=0}^{2}$.
c) Average $\{\tilde{P}_i\}_{i=0}^{2}$ obtaining $\hat{P}_0 = \frac{1}{3}\sum_{i=0}^{2}\tilde{P}_i$.
d) Unfold the average point obtaining $\{\hat{P}_i\}_{i=0}^{2}$.
The centroid ω is marked by $\oplus$.

Algorithm for finding the C_n-symmetry transform:

1. *Fold* the points $\{P_i\}_{i=0}^{n-1}$ by rotating each point P_i counterclockwise about the centroid by $2\pi i/n$ radians (Figure 8b).

2. Let $\hat{P}_0$ be the average of the points $\{\tilde{P}_i\}_{i=0}^{n-1}$ (Figure 8c).

3. *Unfold* the points, obtaining the C_n-symmetric points $\{\hat{P}_i\}_{i=0}^{n-1}$ by duplicating $\hat{P}_0$ and rotating clockwise about the centroid by $2\pi i/n$ radians (Figure 8d).

The set of points $\{\hat{P}_i\}_{i=0}^{n-1}$ is the symmetry transform of the points $\{P_i\}_{i=0}^{n-1}$. i.e. they are the C_n-symmetric configuration of points closest to $\{P_i\}_{i=0}^{n-1}$ in terms of the metric d defined in Section 2 (in terms of the average distance squared). Proof is given in Appendix A.2.

The common case, however, is that shapes have more points than the order of the symmetry. For symmetry of order n, the folding method can be extended to shapes having a number of points which is a multiple of n. A 2D shape P having qn points is represented as q sets $\{S_r\}_{r=0}^{q-1}$ of n interlaced points $S_r = \{P_{rn+i}\}_{i=0}^{n-1}$ (see discussion in Appendix A.4). The C_n-symmetry transform of P (Figure 9) is obtained by applying the above algorithm to each set of n points seperately, where the folding is performed about the centroid of all the points (See Equation 7 in Appendix A.2).

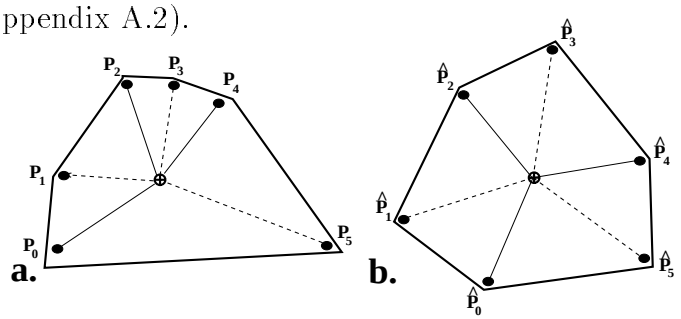

Figure 9: Geometric description of the C_3-symmetry transform for 6 points.
The centroid ω of the points is marked by $\oplus$.
a) The original points shown as 2 sets of 3 points: S_0=$\{P_0, P_2, P_4\}$ and S_1=$\{P_1, P_3, P_5\}$.
b) The obtained C_3-symmetric configuration.

The procedure for evaluating the symmetry transform for mirror-symmetry is similar: Given a shape having $m = 2q$ points we divide the points into q pairs of points (see Appendix A.4) and given an initial guess of the symmetry axis, we apply the folding/unfolding method as follows (see Figure 10):

Algorithm for finding the mirror-symmetry transform:

1. for every pair of points $\{P_0, P_1\}$:
   (a) fold - by reflecting across the mirror symmetry axis obtaining $\{\tilde{P}_0, \tilde{P}_1\}$.
   (b) average - obtaining a single averaged point $\hat{P}_0$.
   (c) unfold - by reflecting back across the mirror symmetry axis obtaining $\{\hat{P}_0, \hat{P}_1\}$.
2. minimize over all possible axis of mirror-symmetry.

The minimization performed in step 2 is, in practice, replaced by an analytic solution (derivation and proof can be found in Appendix A.3).

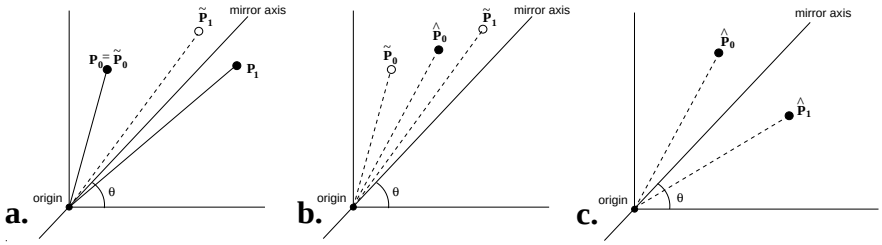

Figure 10: The mirror-symmetry transform of a single pair of points for angle θ, where the centroid of the shape is assumed to be at the origin.
a) The two points $\{P_0, P_1\}$ are folded to obtain $\{\tilde{P}_0, \tilde{P}_1\}$.
b) Points $\tilde{P}_0$ and $\tilde{P}_1$ are averaged to obtain $\hat{P}_0$.
c) $\hat{P}_1$ is obtained by reflecting $\hat{P}_0$ about the symmetry axis.

This method extends to **any** finite point-symmetry group G in **any** dimension, where the folding and unfolding are performed by applying the group elements about the centroid (see derivations in Appendix A.2):

Given a symmetry group G (having n elements) and given a shape P represented by $m = qn$ points, the symmetry transform of the shape with respect to G-symmetry is obtained as follows:

Algorithm for finding the G-symmetry transform:

- The points are divided into q sets of n points.
- For every set of n points:
  - The points are folded by applying the elements of the G-symmetry group.
  - The folded points are averaged, obtaining a single averaged point.
  - The averaged point is unfolded by applying the inverse of the elements of the G-symmetry group. A G-symmetric set of n points is obtained.
- The above procedure is performed over all possible orientations of the symmetry axis and planes of G. Select that orientation which minimizes the Symmetry Distance value. As previously noted, this minimization is analytic in 2D (derivation is given in Appendix A.3) but requires an iterative minimization process in 3D (except for the 3D mirror-symmetry group where a closed form solution has been derived - see [40]).

Figure 11 displays the Symmetry Distance values obtained using the folding method described above with respect to mirror-symmetry, for the shapes shown in Figure 2.

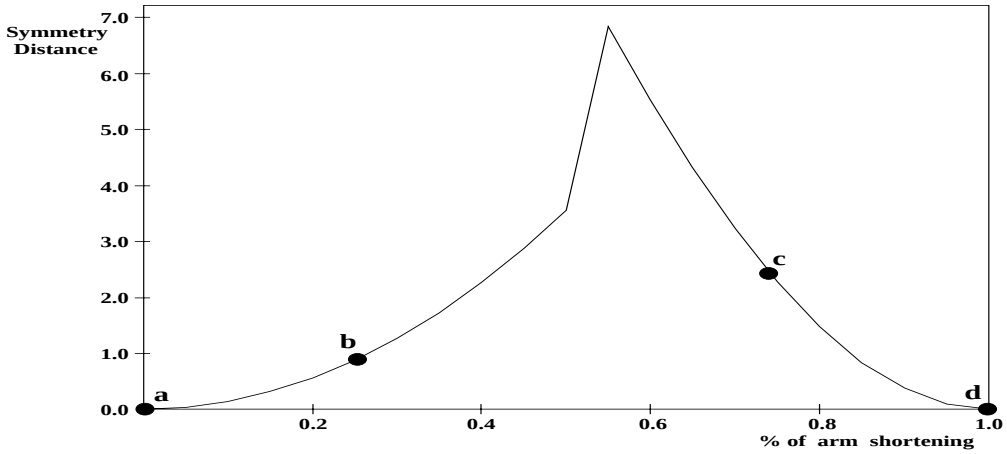

Figure 11: The Symmetry Distance values with respect to mirror symmetry of the shapes of Figure 2 as a function of the percentage of arm shortening. The points a,b,c, and d are the symmetry values obtained for the corresponding shapes in Figure 2.

4 Point Selection for Shape Representation

As symmetry has been defined on a sequence of points, representing a given shape by points must precede the application of the symmetry transform. Selection of points influences the value of SD and depends on the type of object to be measured. If a shape is inherently created from points (such as a graph structure or cyclically connected points creating a polygon) we can represent a shape by these points (Figure 12). This is the case when analysing symmetry of molecules ([44, 43, 40]).

Figure 12: When measuring symmetry of shapes inherently created from points we represent the shape by these points.

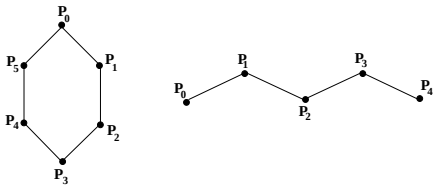

There are several ways to select a sequence of points to represent continuous 2D shapes. One such method is selection at **equal distances**- the points are selected along the shape's contour such that the curve length between every pair of adjacent points is equal (Figure 13).

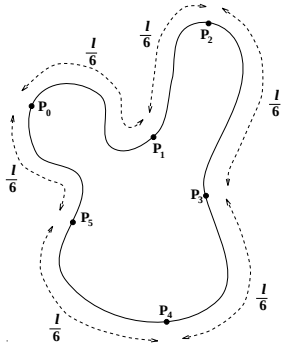

Figure 13: Point selection by equal distance: points are selected along the contour such that each point is equidistant to the next in terms of curve length. In this example six points are distributed along the contour spaced by $\frac{1}{6}$ of the full contour length.

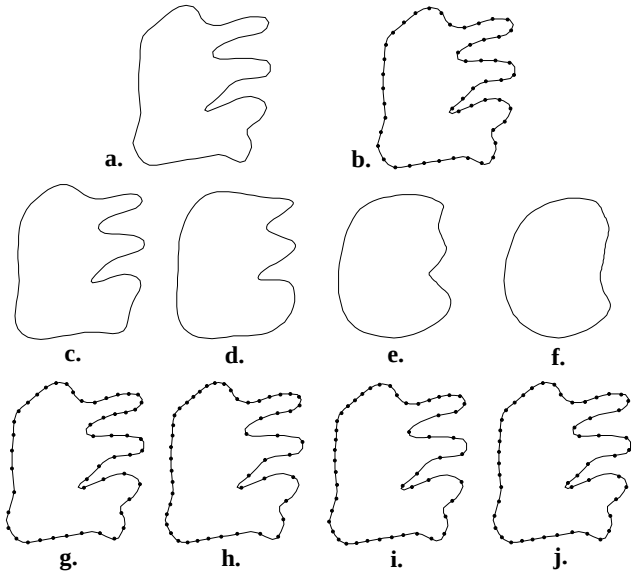

Figure 14: Selection by smoothing
a) Original continuous contour.
b) Points are selected at equal distances along the continuous contour.
c-f) The smoothed shape is obtained by averaging neighboring points of (b). The amount of smoothing depends on the size of the neighborhood. The smoothed shapes (c-f) are obtained when neighborhood includes 5,10,15 and 20 percent of the points, respectively.
g-j) The sampling of points on the original shape using the smoothed shapes (c-f) respectively. Notice that fewer points are selected on the "noisy" part of the contour.

In many cases, however, contour length is not a meaningful measure, as in noisy or occluded shapes. In such cases we propose to select points on a smoothed version of the contour and then project them back onto the original contour. The smoothing of the continuous contour is performed by moving each point on the continuous contour to the centroid of its contour neighborhood. The greater the size of the neighborhood, the greater is the smoothing (see Figure 14). The level of smoothing can vary and for a high level of smoothing, the resulting shape becomes almost a circle about the centroid ([30]).

We use the following procedure for selection by smoothing:
The original contour is first sampled at very high density and at equal distances along the contour obtaining the sampled points $\{M_j\}$ (Figure 15a). Following, each sampled point M_j is replaced by the centroid M'_j of a finite number of its neighboring sampled points. The "smoothed" shape is obtained by connecting the centroid points $\{M'_j\}$ (Figure 15b). A second sampling of points is performed on the smoothed contour, where the points $\{P'_i\}$ are, again, selected at equal distances along the contour. The backprojection is performed by concidering each sampled point P'_i as an interpolated point between two points of the smoothed

shape M'_{j_1} and M'_{j_2} (Figure 15c). The sample point P'_i is backprojected onto the original contour at the point P_i which is the interpolated point between the corresponding sampled points M_{j_1} and M_{j_2} on the original contour (Figure 15d). i.e. $P_i = (P'_i - M_{j_1})\frac{(M_{j_2} - M_{j_1})}{(M'_{j_2} - M'_{j_1})} + M_{j_1}$.

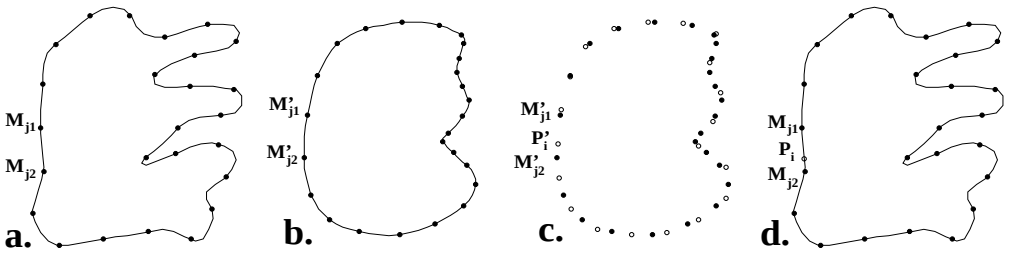

Figure 15: Selection by smoothing (in practice)
a) Continuous contour sampled at equal distances. Points $\{M_j\}$ are obtained.
b) Each sampled point M_j is replaced by the centroid M'_j of a finite number of its neighboring sampled points. The "smoothed" shape is obtained by connecting the centroid points $\{M'_j\}$
c) A second sampling of points is performed at equal distances on the smoothed contour obtaining points $\{P'_i\}$ (white points in Figure). The sample point P'_i is concidered as an interpolation between the two points M'_{j_1} and M'_{j_2}.
d) The sample point P'_i is backprojected onto the original contour at the point P_i which is the interpolated point between the corresponding sampled points M_{j_1} and M_{j_2} on the original contour.

The ultimate smoothing is when the shape is smoothed into a circle. In this case, equal distances on the circular contour is equivalent to equal angles about the center. For maximum smoothing we, therefore, use selection at **equal angles** (Figure 16) where points are selected on the original contour at equal angular intervals around the centroid.

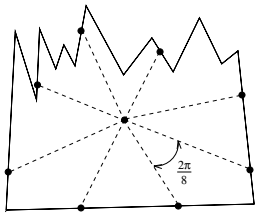

Figure 16: Selection at equal angles: points are distributed along the contour at regular angular intervals around the centroid.

5 Symmetry of Occluded Shapes - Center of Symmetry

When a symmetric object is partially occluded, we use the symmetry distance to evaluate the symmetry of the occluded shapes, locate the center of symmetry and reconstruct the symmetric shape most similar to the unoccluded original.

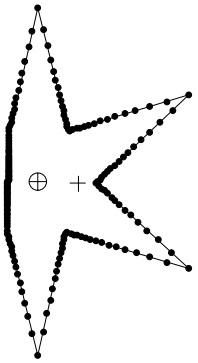

Figure 17: An occluded shape with sampled points selected at equal angles about the center of symmetry (marked by $\oplus$). The symmetry distance obtained using these points is greater than the symmetry distance obtained using points selected at equal angles about the centroid (marked by $+$).

As described in Section 4, a shape can be represented by points selected at regular angular intervals about the centroid. Angular selection of points about a point other than the centroid will give a different symmetry distance value. We define the **center of symmetry** of a shape as that point about which selection at equal angles gives the minimum symmetry distance value. When a symmetric shape is complete the center of symmetry coincides with the centroid of the shape. However, the center of symmetry of truncated or occluded objects does not align with its centroid but is closer to the centroid of the complete shape. Thus the center of symmetry of a shape is robust under truncation and occlusion.

To locate the center of symmetry, we use an iterative procedure of gradient descent that converges from the centroid of an occluded shape to the center of symmetry. Denote by *center of selection*, that point about which points are selected using selection at equal angles. We initialize the iterative process by setting the centroid as the center of selection. At each step we compare the symmetry value obtained from points selected at equal angles about the center of selection with the symmetry value obtained by selection about points in the center of selection's immediate neighborhood. That point about which selection at equal angles gives minimum symmetry value, is set to be the new center of selection. If center of selection does not change, the neighborhood size is decreased. The process is terminated when neighborhood size reaches a predefined minimum size. The center of selection at the end of the process is taken as the center of symmetry.

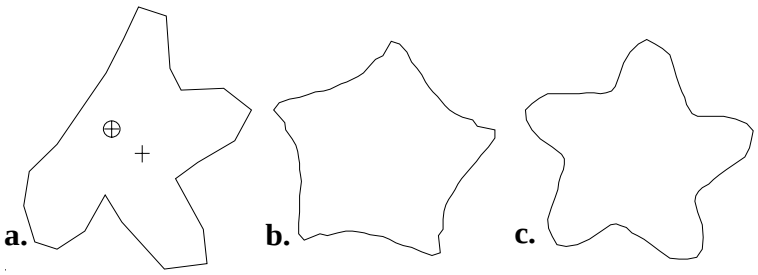

Figure 18: Reconstruction of an occluded shape.
a) Original occluded shape, its centroid (+) and its center of symmetry($\oplus$).
b,c) The closest C_5-symmetric shape following angular selection about the centroid (b) and about the center of symmetry (c). Selection about the centroid gives a featureless shape, while selection about the center of symmetry yields a more meaningful shape.

In the case of occlusions (Figure 18), the closest symmetric shape obtained by angular selection about the center of symmetry is visually more similar to the original than that obtained by angular selection about the centroid. We can reconstruct the symmetric shape closest to the unoccluded shape by obtaining the symmetry transform of the occluded shape using angular selection about the center of symmetry (see Figure 18c). In Figure 19 the center of symmetry and the closest symmetric shapes were found for several occluded flowers.

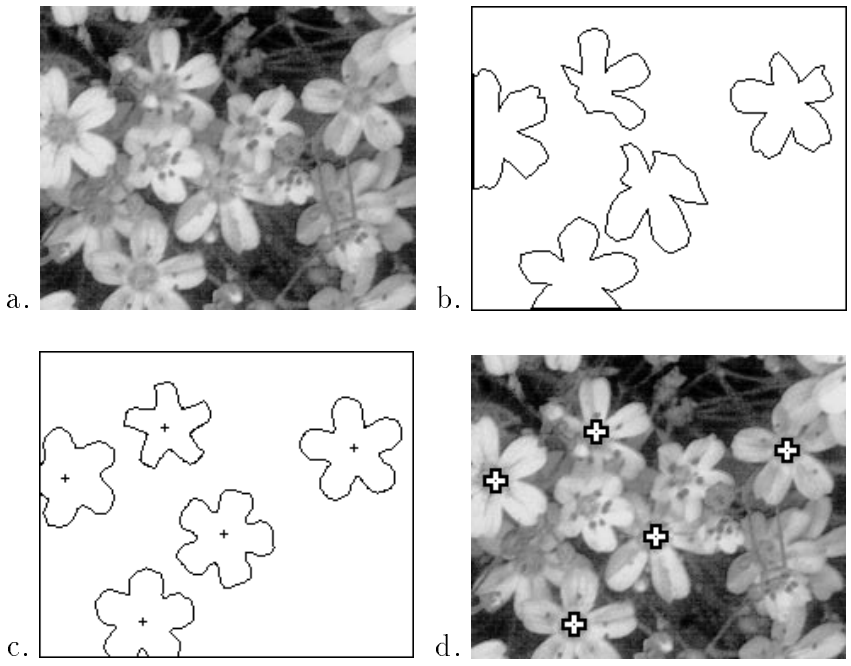

Figure 19: Application example.
a) A collection of occluded asymmetric flowers.
b) Contours of the occluded flowers were extracted manually.
c) The closest symmetric shapes and their center of symmetry.
d) The center of symmetry of the occluded flowers are marked by '+'.

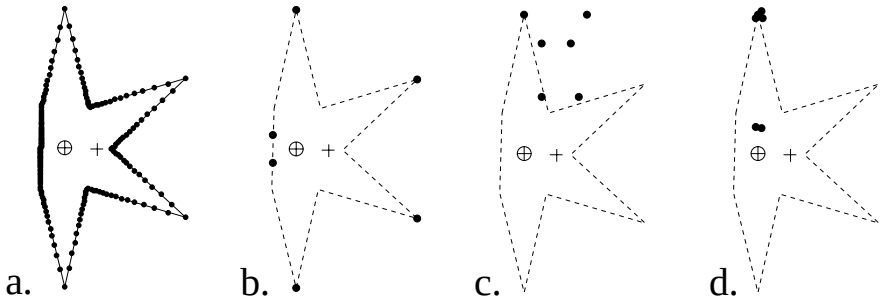

Figure 20: Improving the averaging of folded points
a) An occluded shape with points selected using angular selection about the center of symmetry (marked as $\oplus$).
b) A single set (orbit) of the selected points of a) is shown.
c) folding the points about the centroid (marked as $+$), points are clustered sparsely.
d) folding the points about the center of symmetry, points are clustered tightly. Eliminating the extremes (two farthest points) and averaging results in a smaller averaging error and better reconstruction.

The process of reconstructing the occluded shape can be improved by altering the method of evaluating the symmetry of a set of points. As described in Section 3, the symmetry of a set of points is evaluated by folding, averaging and unfolding about the centroid of the points. We alter the method as follows:

1. The folding and unfolding (steps 1 and 3) will be performed about the center of selection rather than about the centroid of the points.
2. Rather than averaging the folded points (step 2), we apply other robust clustering methods. In practice we average over the folded points, drop the points farthest from the average and then reaverage (see Figure 20).

The improvement in reconstruction of an occluded shape is shown in Figure 21. This method improves both shape and localization of the reconstruction. Assuming that the original shape was symmetric, this method can reconstruct an occluded shape very accurately.

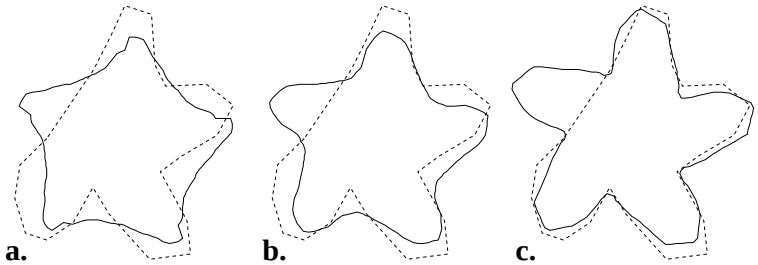

Figure 21: Reconstruction of an occluded almost symmetric shape.
The original shape is shown as a dashed line and the reconstructed shape as a solid line.
a) The closest symmetric shape following angular selection about the centroid.
b) The closest symmetric shape following angular selection about the center of symmetry.
c) The closest symmetric shape following angular selection about the center of symmetry and altered symmetry evaluation (see text).

6 Symmetry of Points with Uncertain Locations

In most cases, sensing processes do not have absolute accuracy and the location of each point in a sensed pattern can be given only as a probability distribution. Given sensed points with such uncertain locations, the following properties are of interest:

- The most probable symmetric configuration represented by the sensed points.
- The probability distribution of symmetry distance values for the sensed points.

6.1 The Most Probable Symmetric Shape

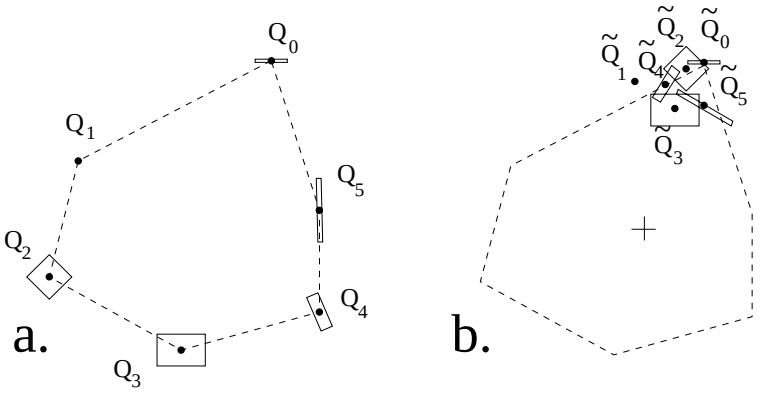

Figure 22: Folding measured points.
a) A configuration of 6 measuremented points $Q_0 \ldots Q_5$. The dot represents the expected location of the point and the rectangle represents the standard deviation marked as rectangles having width and length proportional to the standard deviation.
b) Each measurement Q_i was rotated by $2\pi i/6$ radians about the centroid of the expected point locations (marked as '+') obtaining measurement $\tilde{Q}_0 \ldots \tilde{Q}_5$.

Figure 22a shows a configuration of points whose locations are given by a normal distribution function. The dot represents the expected location of the point and the rectangle represents the standard deviation marked as rectangles having width and length proportional to the standard deviation. In this section we briefly describe a method of evaluating the most probable symmetric shape under the Maximum Likelihood criterion ([13]) given the sensed points. Detailed derivations and proofs are given in Appendix B.1. For simplicity we describe the method with respect to rotational symmetry of order n (C_n-symmetry). The solution for mirror symmetry or any other symmetry is similar (see Appendix B.2).

Given n ordered points in 2D whose locations are given as normal probability distributions with expected location P_i and covariance matrix Λ_i:
$Q_i \sim \mathcal{N}(P_i, \Lambda_i)$ $i = 0 \ldots n-1$, we find the C_n-symmetric configuration of points at locations $\{\hat{P}_i\}_0^{n-1}$ which is optimal under the Maximum Likelihood criterion ([13]).

Denote by ω the centeroid of the most probable C_n-symmetric set of locations $\hat{P}_i$: $\omega = \frac{1}{n}\sum_{i=0}^{n-1}\hat{P}_i$. The point ω is dependent on the location of the measurements (P_i) and on the probability distribution associated with them (Λ_i). Intuitively, ω is positioned at that point about which the folding (described below) gives the tightest cluster of points with small uncertainty (small s.t.d.). We assume for the moment that ω is given. A method for finding ω is derived in Appendix B.1. We use a variant of the folding method which was described in Section 3 for evaluating C_n-symmetry of a set of points:

1. The n measurements $Q_i \sim \mathcal{N}(P_i, \Lambda_i)$ are *folded* by rotating each measurement Q_i by $2\pi i/n$ radians about the point ω. A new set of measurements $\tilde{Q}_i \sim \mathcal{N}(\tilde{P}_i, \tilde{\Lambda}_i)$ is obtained (see Figure 22b).

2. The folded measurements are *averaged* using a weighted average, obtaining a single point $\hat{P}_0$. Averaging is done by considering the n folded measurements $\tilde{Q}_i$ as n measurements of a single point and $\hat{P}_0$ represents the most probable location of that point under the Maximum Likelihood criterion.

$$\hat{P}_0 - \omega = (\sum_{j=0}^{n-1}\tilde{\Lambda}_j^{-1})^{-1}\sum_{i=0}^{n-1}\tilde{\Lambda}_i^{-1}\tilde{P}_i - \omega$$

3. The "average" point $\hat{P}_0$ is *unfolded* as described in Section 3 obtaining points $\{\hat{P}_i\}_{i=0}^{n-1}$ which are perfectly C_n-symmetric.

When we are given $m = qn$ measurements, we find the most probable C_n-symmetric configuration of points, similar to the folding method of Section 3. The m measurements $\{Q_i\}_{i=0}^{m-1}$, are divided into q interlaced sets of n points each, and the folding method as described above is applied seperately to each set of measurements. Derivations and proof of this case is also found in Appendix B.1.

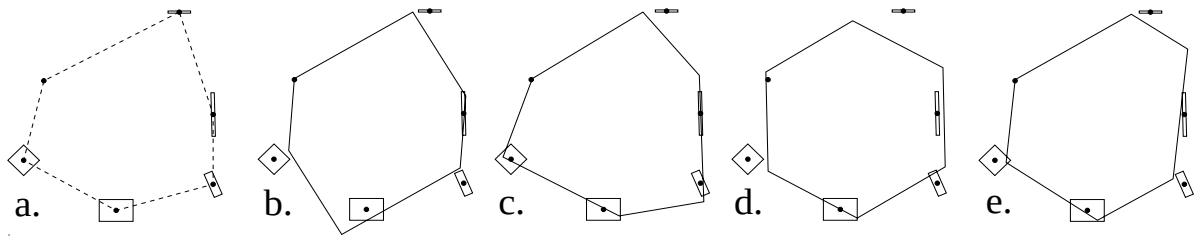

Figure 23: The most probable symmetric shape.
a) A configuration of 6 measured points.
b) The most probable symmetric shapes with respect to C_2-symmetry.
c) The most probable symmetric shapes with respect to C_3-symmetry.
d) The most probable symmetric shapes with respect to C_6-symmetry.
e) The most probable symmetric shapes with respect to mirror-symmetry.

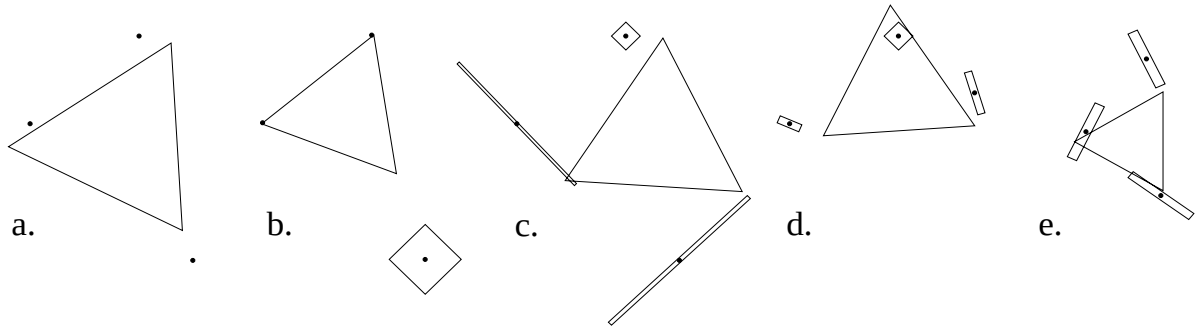

Figure 24: The most probable C_3-symmetric shape for a set of measurements after varying the probability distribution and expected locations of the measurements.
a-c) Changing the uncertainty (s.t.d.) of the measurements.
d-e) Changing both the uncertainty and the expected location of the measurements.

Several examples are shown in Figure 23, where for a given set of measurements, the most probable symmetric shapes were found. Figure 24 shows an example of varying the probability distribution of the measurements on the resulting symmetric shape.

6.2 The Probability Distribution of Symmetry Values

Figure 25a displays a Laue photograph ([2]) which is an interefrence pattern created by projecting X-ray beams onto crystals. Crystal quality is determined by evaluating the symmetry of the pattern. In this case the interesting feature is not the closest symmetric configuration, but the probability distribution of the symmetry distance values.

Consider the configuration of 2D measurements given in Figure 22a. Each measurement Q_i is a normal probability distribution $Q_i \sim \mathcal{N}(P_i, \Lambda_i)$. We assume the centroid of the expectation of the measurements is at the origin. The probability distribution of the symmetry distance values of the original measurements is equivalent to the probability distribution of the location of the "average" point $(\hat{P}_0)$ given the folded measurements as obtained in Step 1 and Step 2 of the algorithm in Section 6.1. It is shown in Appendix B.3 that this probability distribution is a χ^2 distribution of order $n-1$. However, we can approximate the distribution by a gaussian distribution. Details of the derivation are given in Appendix B.3.

In Figure 25 we display distributions of the symmetry distance value as obtained for the Laue photograph given in Figure 25a. In this example we considered every dark patch as a measured point with variance proportional to the size of the patch. Thus in Figure 25b the rectangles which are proportional in size to the corresponding dark patches of Figure 25a, represent the standard deviation of the locations of point measurements. Note that a different

analysis could be used in which the variance of the measurement location is taken as inversely proportional to the size of the dark patch.

a. 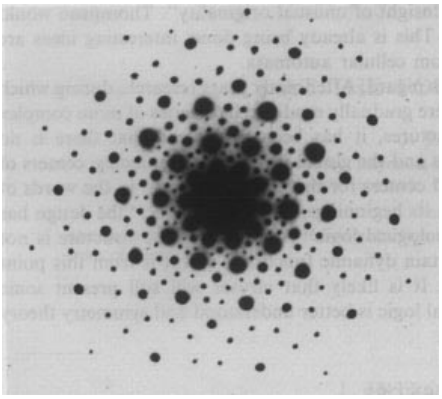

b. 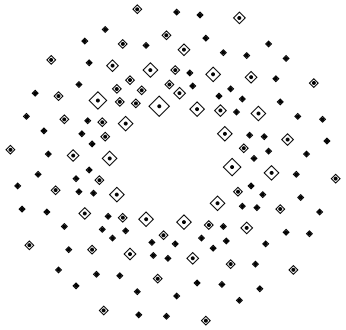

c. 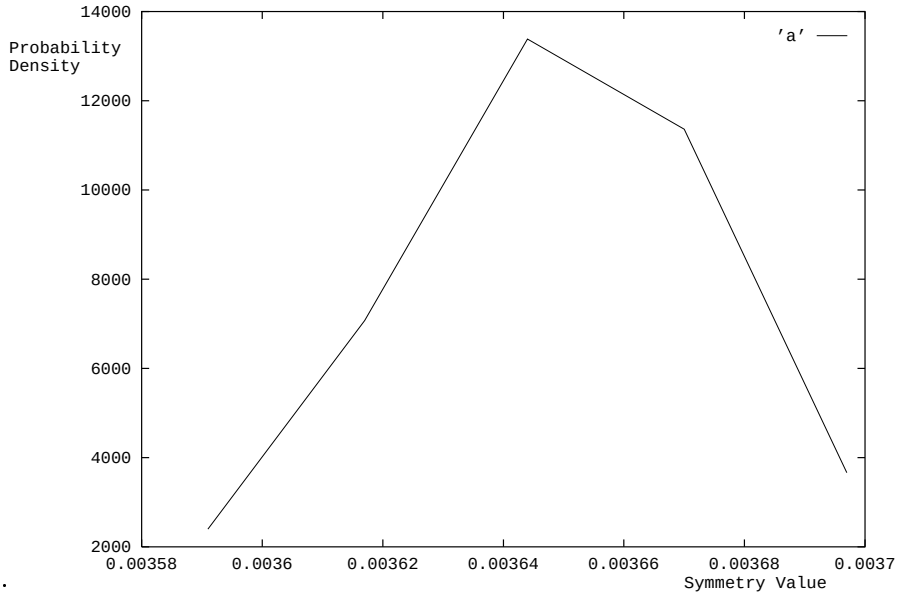

Figure 25: Probability distribution of symmetry values
a) Interference pattern of crystals.
b) Probability distribution of point locations corresponding to a.
c) Probability distribution of symmetry distance values with respect to C_{10}-symmetry was evaluated as described in Appendix B.3. Expectation value = 0.003663.

In Figure 26 we display distributions of the symmetry distance value for various measurements. As expected, the distribution of symmetry distance values becomes broader as the uncertainties (the variance of the distribution) of the measurements increase.

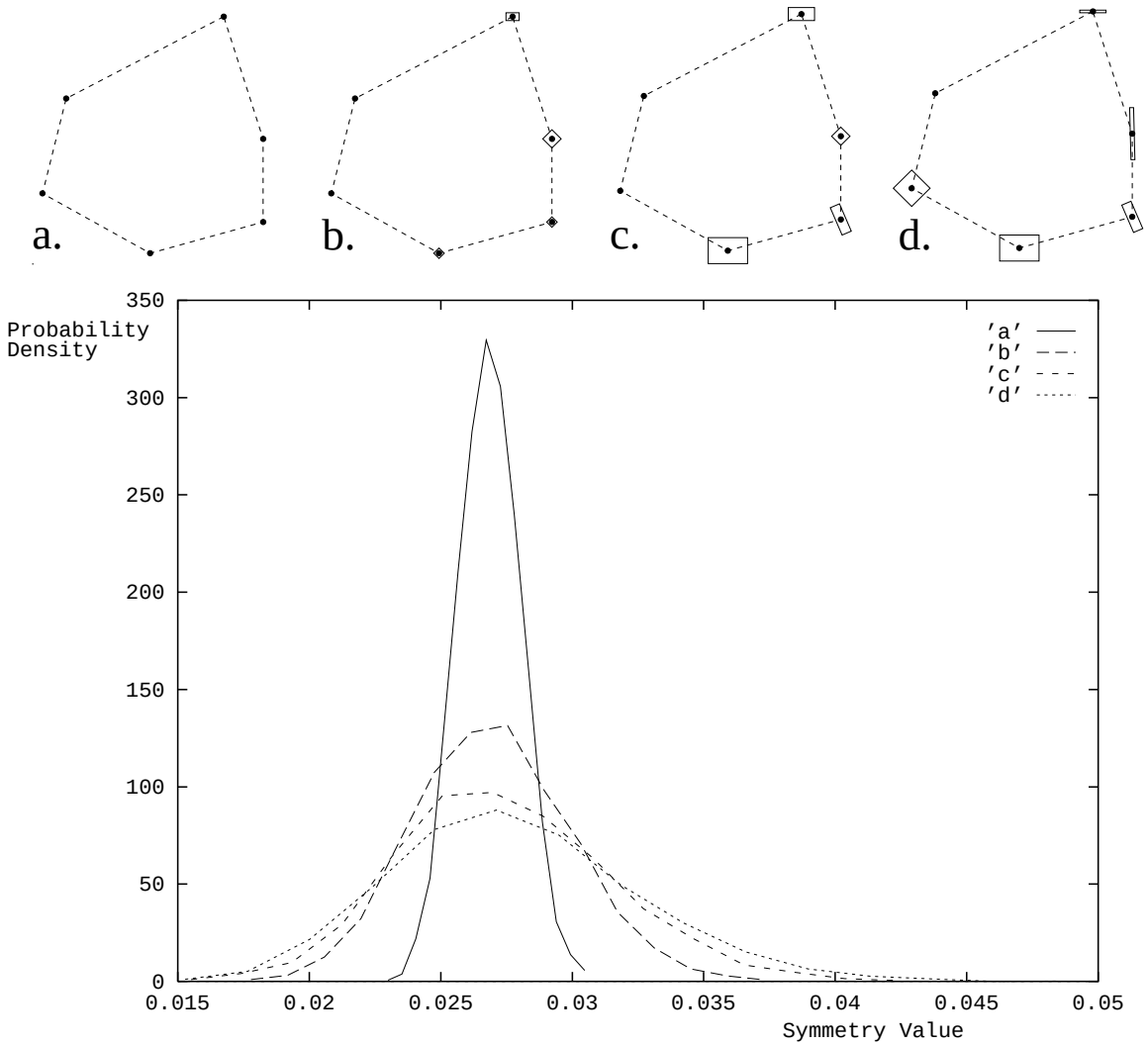

Figure 26: Probability distribution of the symmetry distance value as a function of the variance of the measured points.
a-d) Some examples of configurations of measured points.
e) Probability distribution of symmetry distance values with respect to C_6-symmetry for the configurations a-d.

7 Application to Images

7.1 Finding Orientation of Symmetric 3D Objects

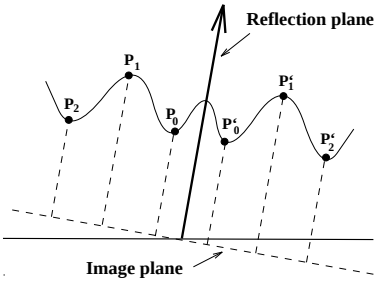

Figure 27: Selecting points on the 3D object (a 2D analog is shown).
For a possible reflection plane, the plane perpendicular to it is sampled. Elevations are recomputed on the object relative to the sampling plane.

When dealing with images, we let pixel values denote elevation, and consider an image as a 3D object on which we can measure 3D symmetries. We applied the SD to find orientation of symmetric 3D objects by finding their 3D mirror-symmetry. The 3D shape is represented by a set of 3D points: for a possible reflection plane, the plane perpendicular to it is sampled. Each sampled points is projected onto the 3D object and its elevation is recomputed relative to the sampling plane (Figure 27). The symmetry value for 3D mirror-symmetry is evaluated using the projected sampling points. The final reflection plane of the 3D object is determined by minimizing the symmetry value over all possible reflection planes. In practice only feasible symmetry planes were tested (i.e. planes which intersect the 3D image) and a gradient descent algorithm was used to increase efficiency of convergence to the minimum symmetry value (the SD). Examples are shown in Figure 28, where a symmetric 3D object is rotated into a frontal vertical view after the refection plane was found.

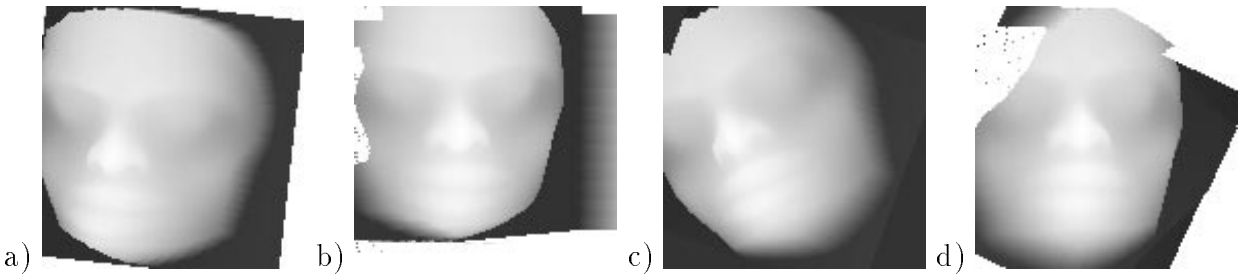

Figure 28: Applying the SD with respect to 3D mirror-symmetry in order to find orientation of a 3D object.
a,c) original depth maps.
b,d) The symmetry reflection plane has been found and the image rotated to a frontal vertical view.

7.2 Using a Multiresolution Scheme

In many images the process of finding the reflection plane did not converge to the correct solution, i.e. the process converged to a local minima due to the sensitivity of the symmetry value to noise and digitization errors. To overcome this problem we introduced a multiresolution scheme, where an initial estimation of the symmetry transform is obtained at low resolution (see Figure 29) and is fine tuned using high resolution images. The solution obtained for the low resolution image is used as an initial guess of the solution for the high resolution image. The low resolution images were obtained by creating gaussian pyramids [12], i.e. convolving the original image with a gaussian.

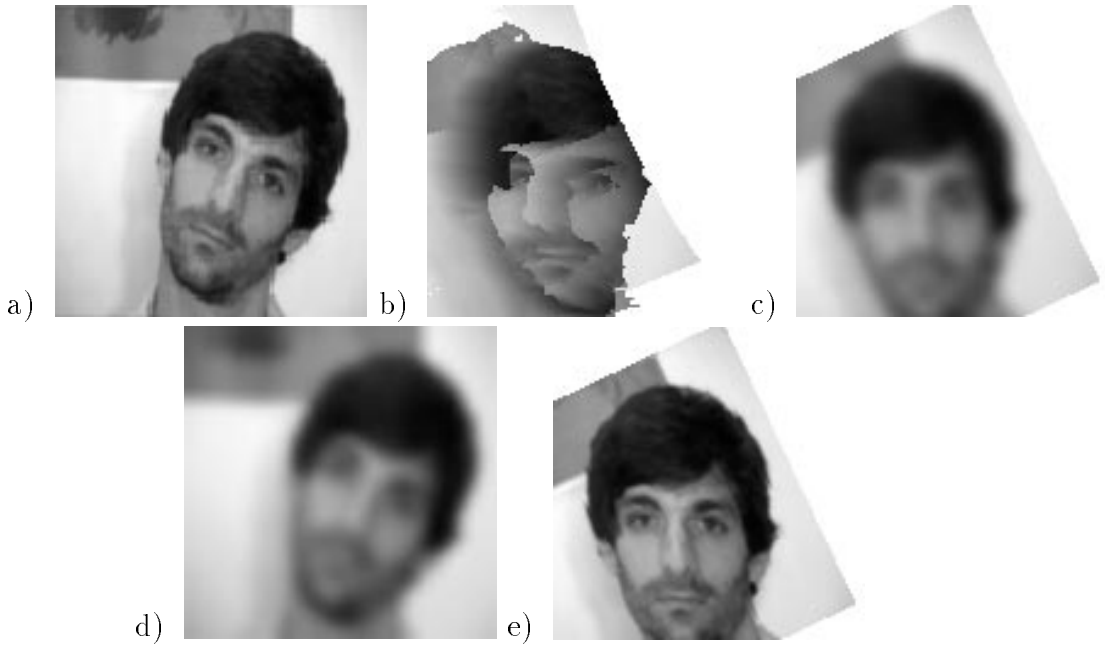

Figure 29: Using multiresolution to find symmetry.
The grey-level image is treated as a depth map and 3D mirror-symmetry is computed. The computed symmetry plane is used to bring the image into a frontal vertical view.
a) Original image.
b) Applying the mirror-symmetry transform on (a) does not find correct reflection plane.
c) A low resolution image obtainined by convolving (a) with a gaussian.
d) Applying the mirror-symmetry transform on the low resolution image (c) gives a good estimation of the reflection plane and direction of gaze.
e) Using the reflection plane found in (d) as an initial guess, the process now converges to the correct symmetry plane.

7.3 Finding Locally symmetric Regions

Most images cannot be assumed to have a single global symmetry, but contain a collection of symmetric and almost symmetric patterns (be they objects or background). We aim to locate these local symmetries and segment the symmetrical objects from the background. The following three staged process is used to extract locally symmetric regions in images.

1. The first stage locates *symmetry focals* - those points about which the image is locally symmetric. Several methods can be used to find the symmetry focals (see [33, 34]). We used a variant of the multiresolution method presented in [41] for sampling and transmitting an image, which uses a simple model of the human visual attention mechanism.

   We used the **Quad Tree** [35] structure which is a hierarchical representation of an image, based on recursive subdivisions of the image array into quadrants as is shown in Figure 30. Every node in the quad tree represents a square region in the image obtained by recursive quadration as follows: the root node of the tree corresponds to the entire image; the four nodes at the next level (if they exist) correspond to the four quadrants of the image and so on; the leaf nodes of the full quad tree correspond to single pixels in the image.

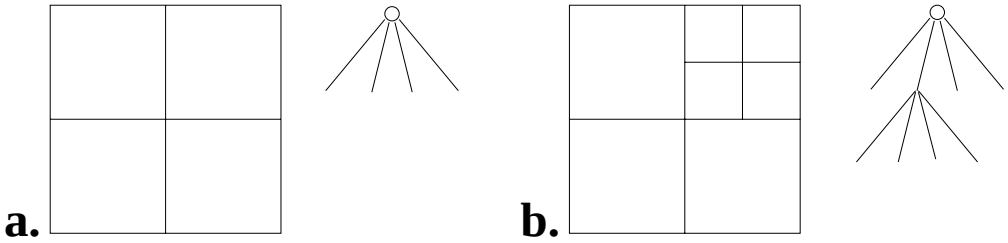

Figure 30: Examples of quad trees. The tessellation of the image is displayed on the left, and the tree representation is on the right.

   The process of locating symmetry focals builds a sequence of quad trees and a sequence of corresponding divisions of the image into quadrants. The process is initialized by setting the current quad tree to a single root node (corresponding to the whole image). At each step all quadrants of the image corresponding to the leaves of the quad tree are tested for a given "interest" function. That node of the quad tree that corresponds to the quadrant with highest "interest" value is selected. The current quad tree is expanded by creating the son nodes of the selected node and accordingly, subdividing

the image quadrant associated with the selected node. Several steps of this procedure are shown in Figure 31. In our case the "interest" function was chosen as to be a function of the Symmetry Distance value obtained for the image quadrant. Thus the procedure described focuses onto regions of high symmetry values and finds symmetry focals. In practice, the "interest" function also took into account the busyness of the image quadrant, thus regions that had low busyness values (i.e. the grey-scale values were almost constant) gave low "interest" values although they were highly symmetric (and gave low Symmetry Distance values). In Figure 32b, a mirror-symmetry focal and an associated reflection plane (passing through the focal) were found.

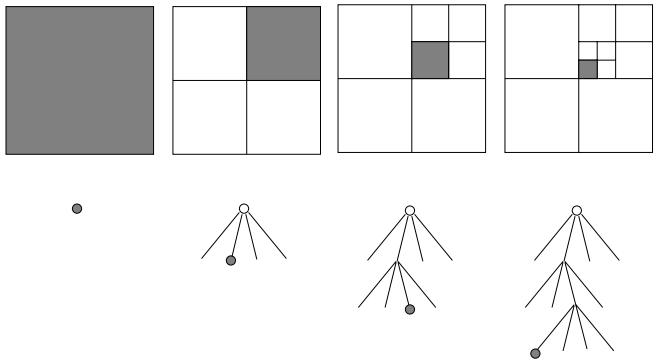

Figure 31: Several steps in the process of finding symmetry focals.
A sequence of quad trees (bottom row) and the corresponding recursive division of the image (top row) is created. The process is initialized by creating a quad tree with a single root node corresponding to the whole image (left). At each step all quadrants of the image corresponding to the leaves of the quad tree are tested for the "interest" function. The leaf of the quad tree that corresponds to the quadrant with highest value (marked in grey) is expanded to create the quad tree of the next step. Three additional steps are shown.

2. Given a symmetry focal and a reflection plane, a symmetry map of the image is created as follows: the original image is sampled at points which are pairwise symmetric with respect to the given reflection plane. The symmetry value obtained using the folding method described in Section 3 for each pair of sampled points is recorded and marked in the symmetry map at the location corresponding to the coordinates of the sampled points. Thus the symmetry map displays the "amount" of mirror-symmetry at every point (with respect to the given reflection plane) where low grey values denote high symmetry content and high grey values denote low symmetry content (Figure 32c).

3. Starting from the symmetry focals, regions are expanded using "active contours" [23] to include compact symmetric regions. The expansion is guided by the symmetry map

and continues as long as the pixels included in the locally symmetric region do not degrade the symmetry of the region more than a predefined threshold (Figure 32d).

a.  b. 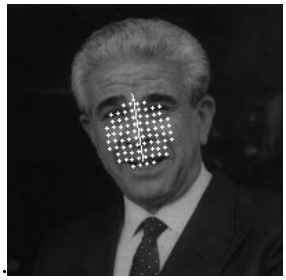 c.  d. 

Figure 32: Applying the Multiresolution scheme to detect a mirror-symmetric region
a) Original image.
b) A mirror-symmetry focal was found.
c) Symmetry map of the image for the mirror-symmetry found in b).
d) Extracted locally symmetric region.

The process can be continued to extract several locally symmetric regions, as shown in the example of Figure 33.

a.  b.  c. 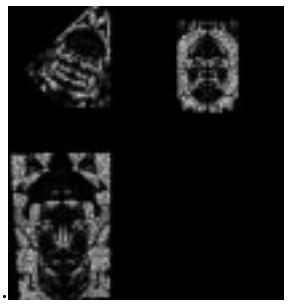 d. 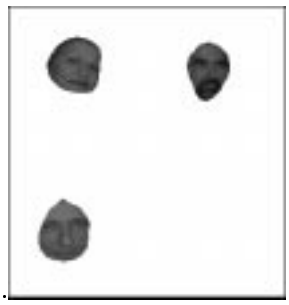

Figure 33: Applying the Multiresolution scheme to find multiple mirror-symmetric regions.
a) Original image.
b) The mirror-symmetry focals found.
c) Symmetry maps of for each mirror-symmetry are merged into a single image.
d) Extracted locally symmetric regions.

8 Conclusion

We view symmetry as a continuous feature and define a Symmetry Distance (SD) of shapes. The general definition of the Symmetry Distance enables a comparison of the "amount" of symmetry of different shapes and the "amount" of different symmetries of a single shape. Furthermore, the SD is associated with the symmetric shape which is 'closest' to the given one, enabling visual evaluation of the SD. Several applications were described including reconstruction of occluded shapes, finding face orientation and finding locally symmetric regions in images. We also described how we deal with uncertain data, i.e. with a configuration of measurements representing the probability distribution of point location. The methods described here can be easily extended to higher dimensions and to more complex symmetry groups. Further extensions will deal with other symmetry classes such as planar symmetry (including translatory symmetry and fractals). Additional work has been done on evaluating reflective symmetry (and chirality) of graph structures ([40, 42]). Current work is expanding the method described here to deal with skewed and projected symmetries.

Appendix

A Mathematical Proof of the Folding Method

In this section we derive mathematically the folding method described in Section 3 for finding the symmetry transform of a shape represented by points.

A.1 Background

We first review some basic definitions required for our proofs and derivations.

A **symmetry group** G is a group whose elements g are matrices representing isometries (distance preserving transformations) in a d dimensional Euclidian space:
$g \in G \;\Rightarrow\; g : \mathcal{R}^d \rightarrow \mathcal{R}^d$
For example, the set of all rotations about the origin in 2D, $\begin{pmatrix} \cos\theta & -\sin\theta \\ \sin\theta & \cos\theta \end{pmatrix}$, is a symmetry group.

A symmetry group having a finite number of elements is a **finite symmetry group**.
For example, the C_3-Symmetry Group is a finite point symmetry group having 3 elements: rotation by 0° (I - identity), rotation by 120° and rotation by 240° about the origin.

A subset of points $S \subset \mathcal{R}^d$ is **G-invariant** if every element of G transforms S onto itself. i.e.: $\{gs \mid s \in S\} = S$ for all $g \in G$.
For example, the set of 2D points $\{(0,1), (\sqrt{3}/2, -1/2), (-\sqrt{3}/2, -1/2)\}$ is C_3-invariant.

The **orbit** of a point $x \in \mathcal{R}^d$ under the symmetry group G is the set of points into which x is transformed using elements of G. i.e.:
$\{gx \mid g \in G\}$.

Given a finite group G and given an ordering of its n elements: $g_0, g_2, \ldots, g_{n-1}$, the **ordered orbit** under G of a point x in Euclidean space is the finite set of points $x_0, \ldots, x_{n-1}$ such that $x_i = g_i x$ for $i = 0 \ldots n-1$. If $g_0 = I$ (the identity element of G) then $x_i = g_i x_0$ $i = 0 \ldots n-1$.

If $S \subset \mathcal{R}^d$ is G-invariant then S is a union of separate orbits. Specifically, an orbit of symmetry group G is itself G-invariant.

A **finite point symmetry group** is a finite symmetry group that has at least one orbit containing a single point. For example the origin is a single point orbit of the C_3-symmetry group described above. Thus the C_3-symmetry group is a finite point symmetry group.

A point $x \in X$ is a **general point** (or is in general position) with respect to G if for all $g \in G, g \neq I$ (where I is the identity in G) we have $gx \neq x$.

Lemma 1 *If G is a finite point symmetry group having n elements and if x is a general point with respect to G, then there are n different points in the orbit of x and all of them are general points.*

Lemma 2 *The centroid of a G-invariant set of points S is a fixed point under G (i.e. the centroid of S is a single point orbit under G).*

Lemma 3 *If S is G-invariant and points $s_1, s_2 \in S$ are fixed points under G, then the translation of the set by the vector $s_2 - s_1$ leaves the set G-invariant (see example in Figure 34).*

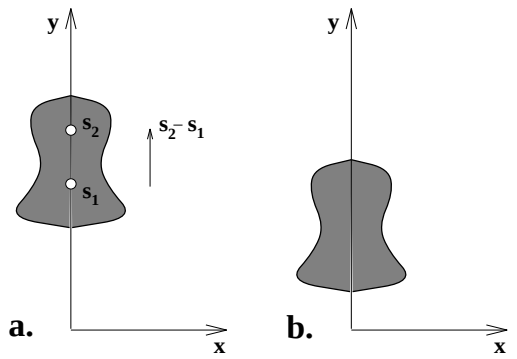

Figure 34: Example of Lemma 3.
a) A set of points in 2D (marked by the hatched area) is mirror-symmetric with the reflection axis coinciding with the y-axis. Points $s_1, s2 \in S$ are fixed points under the mirror symmetry group.
b) Translating the set of points by the vector $s_2 - s_1$ leaves the set mirror symmetric with the reflection axis coinciding with the y-axis.

A subset of points $S \subset \mathcal{R}^n$ is G-**symmetric** if there is a rotation R and a translation vector ω such that the set S' obtained by translating S by t and rotating by R, is G-invariant. $S' = \{R(s - \omega) \mid s \in S\}$.
For example, the set $\{(5+0, 3+1), (5+\sqrt{3}/2, 3-1/2), (5-\sqrt{3}/2, 3-1/2)\}$ in 2D is C_3-symmetric.

For a more detailed review and proofs see [28].

A.2 Proof of the Folding Method

As described in Section 1, the SD of a set of points with respect to a given symmetry group G is evaluated by finding the set of points which is G-symmetric, and which is closest to the given set in terms of the average squared distances. We prove that the folding method of Section 3 indeed finds the closest symmetric set of points.

Given a finite point symmetry group G, we assume without loss of generality that G is centered at the origin (i.e. every element of G leaves the origin fixed). Given an ordering of the n elements of the G-symmetry group $\{g_1 = 0, \ldots, g_{n-1}\}$ and given n general points $P_0, \ldots, P_{n-1}$, we find n points $\hat{P}_0, \ldots, \hat{P}_{n-1}$ and find a rotation matrix R and translation vector w such that the points $\hat{P}_0, \ldots, \hat{P}_{n-1}$ translated by ω and rotated by R form an ordered orbit under G and bring the following expression to a minimum:

$$\sum_{i=0}^{n-1} \|P_i - \hat{P}_i\|^2 \tag{1}$$

Since G has a fixed point at the origin and the centroid of the orbit formed by the rotated and translated $\hat{P}_i$ is a fixed point under G (see Lemma 2), we can assume without loss of generality (from Lemma 3) that the translation vector w is the centroid of points $\hat{P}_i$:

$$w = \frac{1}{n} \sum_{i=0}^{n-1} \hat{P}_i \tag{2}$$

The points $\hat{P}_0, \ldots, \hat{P}_{n-1}$ translated by ω and rotated by R, form an orbit of G, thus the following must be satisfied:

$$\hat{P}_i = R^t g_i R(\hat{P}_0 - w) + w \quad i = 0 \ldots n-1 \tag{3}$$

Using Lagrange multipliers with Equations 1-3 we minimize the following:

$$\sum_{i=0}^{n-1} \|P_i - \hat{P}_i\|^2 \; + \sum_{i=0}^{n-1} \lambda_i^t (\hat{P}_i - R^t g_i R(\hat{P}_0 - w) - w) \; + \varepsilon (w - \frac{1}{n} \sum_{i=0}^{n-1} \hat{P}_i) \tag{4}$$

where ε, λ_i for $i = 0 \ldots n-1$ are the Lagrange multipliers.

Setting the derivatives equal to zero we obtain:

$$\sum_{i=0}^{n-1} (P_i - \hat{P}_i) = 0$$

and using the last constraint (Eq 2) we obtain:

$$w = \frac{1}{n} \sum_{i=0}^{n-1} P_i \tag{5}$$

i.e. the centroid of $P_0, \ldots, P_{n-1}$ coincides with the centroid of $\hat{P}_0, \ldots, \hat{P}_{n-1}$ (in terms of the symmetry distance defined in Section 1, the centroid of a configuration and the centroid of the closest symmetric configuration is the same for any point symmetry group G).

Noting that $R^t g_i R$ for $i = 0 \ldots n-1$ are isometries and distance preserving, we have from the derivatives:

$$\sum_{i=0}^{n-1} R^t g_i^t R(P_i - \hat{P}_i) = 0$$

Expanding using the constraints we obtain:

$$n\hat{P}_0 - n\omega = \sum_{i=0}^{n-1} R^t g_i^t R P_i - \sum_{i=0}^{n-1} R^t g_i^t R w$$

or

$$\hat{P}_0 - w = \frac{1}{n} \sum_{i=0}^{n-1} R^t g_i^t R(P_i - w) \tag{6}$$

The derivation of the rotation matrix R is given in the next section, however, given R, the geometric interpretation of Equation 6 is the folding method, as described in Section 3, proving that the folding method results in the G-symmetric set of points closest to the given set.

The common case, however, is that shapes have more points than the order of the symmetry. For symmetry of order n, the folding method can be extended to shapes having a number of points which is a multiple of n. Given $m = qn$ points (i.e. q sets of n points) $\{P_0^j, \ldots, P_{n-1}^j\}$ $j = 0 \ldots q-1$ we follow the above derivation and obtain a result similar to that given in Equation 6. For each set of n points, i.e. for $j = 0 \ldots q-1$:

$$\hat{P}_0^j - w = \frac{1}{n} \sum_{i=0}^{n-1} R^t g_i^t R(P_i^j - w) \tag{7}$$

where $w = \frac{1}{m} \sum_{j=0}^{q-1} \sum_{i=0}^{n-1} P_i^j$ is the centroid of all m points.
The geometric interpretation of Equation 7 is the folding method, as described in Section 3 for the case of a shape represented by $m = qn$ points.

The folding method for the cases where the number of points is not a multiple of the number of elements in G is not derived here. Details of this case can be found in [43].

A.3 Finding the Optimal Orientation in 2D

Following the derivation in Appendix A.2 we derive here an analytic solution for finding the rotation matrix R which minimizes Equation 4, i.e. finding the orientation of the reflection axes of the G-symmetry group. In [44] (Appendix A.2) we gave the derivation for the specific case of the mirror-symmetry group (D_1) having the two elements: $\{E, \sigma\}$.

In 2D there are 2 classes of point symmetry groups: the class C_n having rotational symmetry of order n and the class D_n having rotational symmetry of order n and n reflection axes (see Section 1.1). The problem of finding the minimizing orientation is irrelevant for the C_n symmetry groups since every element g of these groups is a rotation and $R^t g R = g$. In the case of C_n-symmetry groups, R is usually taken as I (the identity matrix). We derive here a solution for the orientation in the case where G is a D_n symmetry group.

The 2n elements of the D_n-symmetry group $(g_0, \ldots, g_{2n-1})$ can be described as the n elements $g_0 = I, g_1 = R_n^1, g_2 = R_n^2, \ldots, g_{n-1} = R_n^{n-1}$ (where R_n^i is the rotation of $2\pi/n$ radians about the origin) and the n elements obtained by applying a reflection R_f on each of these elements: $g_n = R_f, g_{n+1} = R_f R_n^1, g_{n+2} = R_f R_n^2, \ldots, g_{2n-1} = R_f R_n^{n-1}$. We denote the orientation of the symmetry group as the angle θ between the reflection axis and the y axis. Thus

$$R = \begin{pmatrix} \cos\theta & \sin\theta \\ -\sin\theta & \cos\theta \end{pmatrix}$$

and the reflection operation R_f is given by:

$$R_f = R^t g_{n+1} R = \begin{pmatrix} \cos\theta & -\sin\theta \\ \sin\theta & \cos\theta \end{pmatrix} \begin{pmatrix} -1 & 0 \\ 0 & 1 \end{pmatrix} \begin{pmatrix} \cos\theta & \sin\theta \\ -\sin\theta & \cos\theta \end{pmatrix} = \begin{pmatrix} -\cos 2\theta & -\sin 2\theta \\ -\sin 2\theta & \cos 2\theta \end{pmatrix}$$

Without loss of generality, we assume the centroid w is at the origin ($\omega = 0$). Following Appendix A.2, we minimize Equation 1 over θ. Using Equation 3 and noting that $R^t g_i R$ for $i = 0 \ldots 2n-1$ are distance preserving, we minimize the following over θ:

$$\sum_{i=0}^{2n-1} \|P_i - \hat{P}_i\|^2 \;=\; \sum_{i=0}^{2n-1} \|R^t g_i^t R P_i - \hat{P}_0\|^2$$

Substituting Equation 6 we minimize:

$$\sum_{i=0}^{2n-1} \|R^t g_i^t R P_i - \frac{1}{2n} \sum_{j=0}^{2n-1} R^t g_j^t R P_j\|^2$$

Rearranging and noting that $R^t g_i^t R = g_i^t$ for $i = 0 \ldots n-1$, we minimize:

$$\sum_{i=0}^{2n-1} \|2n R^t g_i^t R P_i - \sum_{j=0}^{n-1} g_j^t P_j - \sum_{j=n}^{2n-1} R_f g_{j-n}^t P_j\|^2 \qquad (8)$$

Denoting by x_i, y_i the coordinates of the point P_i and taking the derivative of Equation 8 with respect to θ we obtain:

$$\tan 2\theta = \frac{\sum_{i=0}^{n-1} \sum_{j=n}^{2n-1} (x_i y_j + x_j y_i)}{\sum_{i=0}^{n-1} \sum_{j=n}^{2n-1} (x_i x_j - y_i y_j)} \tag{9}$$

which is an analytic solution for the case of optimal orientation in 2D. In higher dimensions, however, no analytic solution was found and a minimization procedure is used (except for the mirror symmetry group in 3D where a closed form solution is given - see [42]).

A.4 Dividing Points of a Shape into sets

As described in Section 3, when measuring C_n-symmetry (rotational symmetry of order n) of a shape represented by a multiple of n points, the points must be divided into sets of n points. In general, this problem is exponential, however when the points are ordered along a contour, as in our case, the possible divisions into sets are more restricted since the ordering is preserved under the symmetry transform of a shape. For example, points in 2D along the contour of a C_n-symmetric shape form orbits which are interlaced. An example is shown in Figure 35a for C_3-symmetry. where 3 interlaced orbits are shown marked as $\bullet$, $\circ$ and $\square$. Thus, given a set of $m = nq$ ordered points there is only one possible division of the points into q sets of n points such that the ordering is preserved in the symmetric shape - the q sets must be interlaced (as was shown in Figure 9). In the case of D_n-symmetry (rotational and reflective symmetry of order n) the $m = 2nq$ ordered points, form q orbits which are interlaced and partially inverted to account for the reflection symmetry. An example is shown in Figure 35b for D_4-symmetry where instead of 3 interlaced orbits $\bullet \circ \square \bullet \circ \square \ldots \bullet \circ \square \bullet \circ \square$, every other run is inverted: $\bullet \circ \square\square \circ \bullet \ldots \bullet \circ \square\square \circ \bullet$. Thus, given a set of $m = 2nq$ ordered points there are $m/2n = q$ possible division of the points.

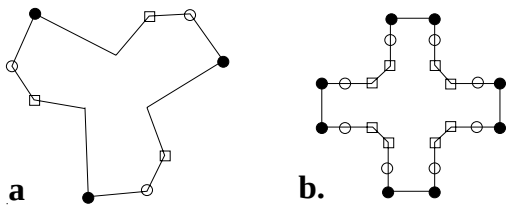

Figure 35: Dividing m selected points into interlaced sets:
a) C_n-symmetry - 1 possibility.
b) D_n-symmetry - $m/2n$ possibilities

B Uncertain Point Locations

B.1 The most Probable C_n-Symmetric Shape

In Section 6.1 we described a method of evaluating the most probable symmetric shape given a set of measurements. In this Section we derive mathematically and prove the method. For simplicity we derive the method with respect to rotational symmetry of order n (C_n-symmetry). The solution for mirror symmetry is similar (see Appendix B.2).

Given n points in 2D whose positions are given as normal probability distributions: $Q_i \sim \mathcal{N}(P_i, \Lambda_i), \quad i = 0 \ldots n-1$, we find the C_n-symmetric configuration of points $\{\hat{P}_i\}_0^{n-1}$ which is most optimal under the Maximum Likelihood criterion ([13]).

Denote by ω the center of mass of $\hat{P}_i$: $\quad \omega = \frac{1}{n}\sum_{i=0}^{n-1} \hat{P}_i$.

Having that $\{\hat{P}_i\}_0^{n-1}$ are C_n-symmetric, the following is satisfied:

$$\hat{P}_i = R_i(\hat{P}_0 - \omega) + \omega \tag{10}$$

for $i = 0 \ldots \quad n-1$ where R_i is a matrix representing a rotation of $2\pi i/n$ radians.

Thus, given the measurements $Q_0, \ldots, Q_{n-1}$ we find the most probable $\hat{P}_0$ and ω. We find $\hat{P}_0$ and ω that maximize $\mathrm{Prob}(\{\mathrm{P_i}\}_{\mathrm{i=0}}^{\mathrm{n-1}} \mid \omega, \hat{\mathrm{P}}_0)$ under the symmetry constraints of Equation 10.

Considering the normal distribution we have:

$$\prod_{i=0}^{n-1} k_i \exp(-\frac{1}{2}(\hat{P}_i - P_i)^t \Lambda_i^{-1}(\hat{P}_i - P_i)$$

where $k_i = \frac{1}{2}\pi \mid \Lambda_i \mid^{1/2}$. Having log being a monotonic function, we maximize:

$$\log \prod_{i=0}^{n-1} k_i \exp(-\frac{1}{2}(\hat{P}_i - P_i)^t \Lambda_i^{-1}(\hat{P}_i - P_i)$$

Thus we find those parameters which maximize:

$$-\frac{1}{2}\sum_{i=0}^{n-1}(\hat{P}_i - P_i)^t \Lambda_i^{-1}(\hat{P}_i - P_i)$$

under the symmetry constraint of Equation 10.

Substituting Equation 10, taking the derivative with respect to $\hat{P}_0$ and equating to zero we obtain:

$$\underbrace{(\sum_{i=0}^{n-1} R_i^t \Lambda_i^{-1} R_i)}_{A}\hat{P}_0 + \underbrace{\sum_{i=0}^{n-1} R_i^t \Lambda_i^{-1}(I - R_i)}_{B}\omega \;\; = \underbrace{\sum_{i=0}^{n-1} R_i^t \Lambda_i^{-1} P_i}_{E} \tag{11}$$

Note that $R_0 = I$ where I is the identity matrix.

When the derivative with respect to ω is zero:

$$\underbrace{(\sum_{i=0}^{n-1}(I-R_i)^t\Lambda_i^{-1}R_i)}_{C}\hat{P}_0+\underbrace{\sum_{i=0}^{n-1}(I-R_i)^t\Lambda_i^{-1}(I-R_i)}_{D}\omega=\underbrace{\sum_{i=0}^{n-1}(I-R_i)^t\Lambda_i^{-1}P_i}_{F} \tag{12}$$

Notice that when all Λ_i are equal (i.e. all points have the same uncertainty, which is equivalent to the cases in the previous sections where point location is known with no uncertainty), Eqs. 11-12 reduce to Eqs. 5-6 in Appendix A.2.

From Equation 11 we obtain

$$\hat{P}_0-\omega=(\sum_{j=0}^{n-1}R_j^t\Lambda_j^{-1}R_j)^{-1}\sum_{i=0}^{n-1}(R_i^t\Lambda_i^{-1}R_i)R_i^tP_i$$

Which gives the folding method described in Section 6.1, where $R_i^tP_i$ is the location of the folded measurement (denoted $\tilde{P}_i$ in the text) and $R_i^t\Lambda_i^{-1}R_i$ is its probability distribution (denoted $\tilde{\Lambda}_i$ in the text). The factor $(\sum_{j=0}^{n-1}R_j^t\Lambda_j^{-1}R_j)$ is the normalization factor.

Reformulating Eqs. 11 and 12 in matrix formation we obtain:

$$\underbrace{\begin{pmatrix}A & B\\ C & D\end{pmatrix}}_{U}\underbrace{\begin{pmatrix}\hat{P}_0\\ \omega\end{pmatrix}}_{V}=\underbrace{\begin{pmatrix}E\\ F\end{pmatrix}}_{Z}$$

Noting that U is symmetric we solve by inversion $V=U^{-1}Z$ obtaining the parameters ω,$\hat{P}_0$ and obtaining the most probable C_n-symmetric configuration, given the measurements $\{Q_i\}_{i=0}^{n-1}$.

Similar to the representation in Section 3, given $m=qn$ measurements $\{Q_i\}_{i=0}^{m-1}$, we consider them as q sets of n interlaced measurements: $\{Q_{iq+j}\}_{i=0}^{n-1}$ for $j=0\ldots q-1$. The derivations given above are applied to each set of n measurements separately, inorder to obtain the most probable C_n-symmetric set of points $\{\hat{P}_i\}_{i=0}^{m-1}$. Thus the symmetry constraints that must be satisfied are:

$$\hat{P}_{iq+j}=R_i(\hat{P}_j-\omega)+\omega$$

for $j=0\ldots\ q-1$ and $i=0\ldots\ n-1$ where, again, R_i is a matrix representing a rotation of $2\pi i/n$ radians and ω is the centroid of all points $\{\hat{P}_i\}_{i=0}^{m-1}$.

As derived in Equation 11, we obtain for $j=0\ldots q-1$:

$$\underbrace{(\sum_{i=0}^{n-1}R_i^t\Lambda_{iq+j}^{-1}R_i)}_{A_j}\hat{P}_j+\underbrace{\sum_{i=0}^{n-1}R_i^t\Lambda_{iq+j}^{-1}(I-R_i)}_{B_j}\omega=\underbrace{\sum_{i=0}^{n-1}R_i^t\Lambda_{iq+j}^{-1}P_{iq+j}}_{E_j} \tag{13}$$

and equating to zero, the derivative with respect to ω, we obtain, similar to Equation 12:

$$\sum_{j=0}^{q-1}\underbrace{(\sum_{i=0}^{n-1}(I-R_i)^t\Lambda_{iq+j}^{-1}R_i)}_{C_j}\hat{P}_j+\underbrace{\sum_{j=0}^{q-1}\sum_{i=0}^{n-1}(I-R_i)^t\Lambda_{iq+j}^{-1}(I-R_i)}_{D}\omega=\underbrace{\sum_{j=0}^{q-1}\sum_{i=0}^{n-1}(I-R_i)^t\Lambda_{iq+j}^{-1}P_{iq+j}}_{F} \tag{14}$$

Reformulating Eqs. 13 and 14 in matrix formation we obtain:

$$\underbrace{\begin{pmatrix} A_0 & & & B_0 \\ & A_1 & & B_1 \\ & & \ddots & \vdots \\ & & A_{q-1} & B_{q-1} \\ C_0 & C_1 & \cdots C_{q-1} & D \end{pmatrix}}_{U} \underbrace{\begin{pmatrix} \hat{P}_0 \\ \hat{P}_1 \\ \vdots \\ \hat{P}_{q-1} \\ \omega \end{pmatrix}}_{V} = \underbrace{\begin{pmatrix} E_0 \\ E_1 \\ \vdots \\ E_{q-1} \\ F \end{pmatrix}}_{Z}$$

Noting that U is symmetric we solve by inversion $V = U^{-1}Z$ and obtain the parameters ω and $\{\hat{P}_j\}_{j=0}^{q-1}$, and obtain the most probable C_n-symmetric configuration, $\{\hat{P}_j\}_{j=0}^{m-1}$ given the measurements $\{Q_i\}_{i=0}^{m-1}$.

B.2 The Most Probable Mirror Symmetric Shape

In Section 6.1 we described a method for finding the most probable rotationaly symmetric shape given measurements of point location. The solution for mirror symmetry is similar. In this case, given m measurements (where $m = 2q$), the unknown parameters are $\{\hat{P}_j\}_{j=0}^{q-1}, \omega$ and θ where θ is the angle of the reflection axis. However these parameters are redundant and we reduce the dimensionality of the problem by replacing the 2 dimensional ω with the one dimensional x_0 representing the x-coordinate at which the reflection axis intersects the x-axis. Additionally we replace R_i the rotation matrix with $R = \begin{pmatrix} \cos 2\theta & \sin 2\theta \\ \sin 2\theta & -\cos 2\theta \end{pmatrix}$ the reflection about an axis at an angle θ to the x-axis. The angle θ is found analyticaly (see [44]) thus the dimensionality of the problem is $2q + 1$ (rather than $2q + 2$) and elimination of the last row and column of matrix U (see Section 6.1) allows an inverse solution as in the rotational symmetry case.

B.3 Probability Distribution of Symmetry Values

In this section we derive mathematically the probability distribution of symmetry distance values obtained from a set of n measurements in 2D: $Q_i \sim \mathcal{N}(P_i, \Lambda_i) \quad i = 0 \ldots n-1$ with respect to C_n-symmetry (see Section 6.2).

Denote by X_i the 2-dimensional random variable having a normal distribution equal to that of measurement $\tilde{Q}_i$ i.e.

$$\begin{aligned} E(X_i) &= R_i P_i \\ \mathrm{Cov}(X_i) &= R_i \Lambda_i R_i^t \end{aligned}$$

where R_i denotes (as in Section 3) the rotation matrix of $2\pi i/n$ radians.

Denote by Y_i the 2-dimensional random variable:

$$Y_i = X_i - \frac{1}{n}\sum_{j=0}^{n-1} X_j$$

in matrix notation:

$$\underbrace{\begin{pmatrix} Y_0 \\ \vdots \\ Y_{n-1} \end{pmatrix}}_{\mathbf{Y}} = A \underbrace{\begin{pmatrix} X_0 \\ \vdots \\ X_{n-1} \end{pmatrix}}_{\mathbf{X}}$$

or $\mathbf{Y} = A\mathbf{X}$ where $\mathbf{Y}$ and $\mathbf{X}$ are of dimension $2n$ and A is the $2n \times 2n$ matrix:

$$A = \frac{1}{n}\begin{pmatrix} n-1 & 0 & -1 & 0 & -1 & \cdots \\ 0 & n-1 & 0 & -1 & 0 & \cdots \\ -1 & 0 & \ddots & 0 & -1 & \cdots \\ & & & \ddots & & \\ & & & & \ddots & \\ & & & \cdots & & n-1 \end{pmatrix}$$

And we have

$$E(\mathbf{X}) = \begin{pmatrix} E(X_0) \\ \vdots \\ E(X_{n-1}) \end{pmatrix} \quad \mathrm{Cov}(\mathbf{X}) = \begin{pmatrix} \mathrm{Cov}(X_0) & & \\ & \ddots & \\ & & \mathrm{Cov}(X_{n-1}) \end{pmatrix}$$

$$E(\mathbf{Y}) = AE(\mathbf{X}) \qquad \mathrm{Cov}(\mathbf{Y}) = A\mathrm{Cov}(\mathbf{X})A^t$$

The matrix $A\mathrm{Cov}(\mathbf{X})A^t$, being symmetric and positive definite, we find the $2n \times 2n$ matrix S diagonalizing $\mathrm{Cov}(\mathbf{Y})$ i.e.

$$SA\mathrm{Cov}(\mathbf{X})A^tS^t = D$$

where D is a diagonal matrix (of rank $2(n-1)$).

Denote by $\mathbf{Z} = (Z_0, \ldots, Z_{n-1})^t$ the $2n$-dimensional random variable $SA\mathbf{X}$.

$$\begin{aligned} E(\mathbf{Z}) &= SAE(\mathbf{X}) \\ \mathrm{Cov}(\mathbf{Z}) &= SA\mathrm{Cov}(\mathbf{X})A^tS^t = D \end{aligned}$$

Thus the random variables Z_i that compose $\mathbf{Z}$ are independent and, being linear combinations of X_i, they are of normal distribution.

The symmetry distance, as defined in Section 3, is equivalent, in the current notations, to $s = \mathbf{Y}^t\mathbf{Y}$. Having S orthonormal we have

$$s = (SA\mathbf{X})^tSA\mathbf{X} = \mathbf{Z}^t\mathbf{Z}$$

If $\mathbf{Z}$ were a random variable of standard normal distribution, we would have s being of a χ^2 distribution of order $2(n-1)$. In the general case Z_i are normally distributed but not standard and $\mathbf{Z}$ cannot be standardized globally. We approximate the distribution of s as a normal distribution with

$$\begin{aligned} E(s) &= E(\mathbf{Z})^tE(\mathbf{Z}) + \mathrm{trace}D^tD \\ \mathrm{Cov}(s) &= 2\mathrm{trace}(D^tD)(D^tD) + 4E(\mathbf{Z})^tD^tDE(\mathbf{Z}) \end{aligned}$$

References

[1] H. Alt, K. Mehlhorn, H. Wagener, and E. Welzl. Congruence, similarity and symmetries of geometric objects. *ACM Journal of Computing*, 4:308–315, 1987.

[2] J.L. Amoros, M.J. Buerger, and M.Canut de Amoros. *The Laue Method.* Academic Press, New York, 1975.

[3] M. Atallah. On symmetry detection. *IEEE Trans. on Computers*, c-34(7):663–666, 1985.

[4] F. Attneave. Symmetry information and memory for patterns. *American Journal of Psychology*, 68:209–222, 1955.

[5] D. Avnir and A.Y. Meyer. Quantifying the degree of molecular shape deformation. a chirality measure. *Journal of Molecular Structure (Theochem)*, 94:211–222, 1991.

[6] J. Bigün. Recognition of local symmetries in gray value images by harmonic functions. In *9-ICPR*, pages 345–347, 1988.

[7] J. Bigün and G. Granlund. Optimal orientation detection of linear symmetry. In *First International Conference on Computer Vision*, pages 433–438, London, June 1987.

[8] A. Blake, M. Taylor, and A. Cox. Grasping visual symmetry. In *International Conference on Pattern Recognition*, pages 724–733, Berlin, May 1993.

[9] H. Blum and R.N. Nagel. Shape description using weighted symmetric axis features. *Pattern Recognition*, 10:167–180, 1978.

[10] Y. Bonneh, D. Reisfeld, and Y. Yeshurun. Texture discrimination by local generalized symmetry. In *International Conference on Pattern Recognition*, pages 461–465, Berlin, May 1993.

[11] M. Brady and H. Asada. Smoothed local symmetries and their implementation. *Int. J. Robotics Research*, 3(3):36–61, 1984.

[12] P. Burt and E.H. Adelson. The Laplacian pyramid as a compact image code. *IEEE Trans. on Communications*, COM-31:532–540, 1983.

[13] M. H. DeGroot. *Probability and Statistics.* Addison-Wesley, Reading, MA, 1975.

[14] J.M. Dinten. Tomographic reconstruction of axially symmetric objects: Regularization by a markovian modelization. In *International Conference on Pattern Recognition*, volume 2, pages 153–158, 1990.

[15] M. Fleck. Local rotational symmetries. In *IEEE Conference on Computer Vision and Pattern Recognition*, pages 332–337, 1986.

[16] G. Gilat. Chiral coefficient - a measure of the amount of structural chirality. *J. Phys. A: Math. Gen.*, 22:545–545, 1989.

[17] B. Grünbaum. Measures of symmetry for convex sets. *Proc. Symp. Pure Math: American Mathematical Society*, 7:233–270, 1963.

[18] Y. Hel-Or, S. Peleg, and D. Avnir. Characterization of right handed and left handed shapes. *CVGIP:Image Understanding*, 53(2), 1991.

[19] P.T. Highnam. Optimal algorithms for finding the symmetries of planar point sets. *Information Processing Letters*, 22:219–222, 1986.

[20] M-K. Hu. Visual pattern recognition by moment invariants. *IRE Transactions on Information Theory*, IT-20:179–187, Feb 1962.

[21] J.Ponce. On characterizing ribbons and finding skewed symmetries. *Computer Vision, Graphics, and Image Processing*, 52:328–340, 1990.

[22] B. Julesz and Chang. Symmetry perception and spatial frequency channels. *Perception*, 8:711–718, 1979.

[23] M. Kass, A. Witkin, and D. Terzopoulos. Snakes: active contour models. *International Journal of Computer Vision*, 1:322–332, 1988.

[24] M. Kirby and L. Sirovich. Application of the karhunen-loeve procedure for the characterization of human faces. *IEEE Trans. on Pattern Analysis and Machine Intelligence*, 12(1):103–108, 1990.

[25] M. Leyton. *Symmetry, Causality, Mind*. MIT press, Cambridge, MA, 1992.

[26] P. Locher and C. Nodine. Influence of stimulus symmetry on visual scanning patterns. *Perception and Psychophysics*, 13(3):408–412, 1973.

[27] G. Marola. On the detection of the axes of symmetry of symmetric and almost symmetric planar images. *IEEET-PAMI*, 11(1):104–108, 1989.

[28] W. Miller. *Symmetry Groups and their Applications*. Academic Press, London, 1972.

[29] H. Mitsumoto, S. Tamura, K. Okazaki, N. Kajimi, and Y. Fukui. 3-d reconstruction using mirror images based on a plane symmetry recovering method. *IEEE Trans. on Pattern Analysis and Machine Intelligence*, 14(9):941–946, 1992.

[30] F. Mokhatarian and A. Mackworth. A theory of multiscale, curvature-based shape representation for planar curves. *IEEE Trans. on Pattern Analysis and Machine Intelligence*, 14:789–805, 1992.

[31] W.G. Oh, M. Asada, and S. Tsuji. Model based matching using skewed symmetry information. In *9-ICPR*, pages 1043–1045, 1988.

[32] D. Reisfeld, H. Wolfson, and Y. Yeshurun. Detection of interest points using symmetry. In *Proc. of the 7th Israeli Symposium on Artificial Intelligence and Computer Vision*, pages 339–348, 1990.

[33] D. Reisfeld, H. Wolfson, and Y. Yeshurun. Detection of interest points using symmetry. In *International Conference on Computer Vision*, pages 62–65, 1992.

[34] D. Reisfeld, H. Wolfson, and Y. Yeshurun. Robust facial feature detection using local symmetry. In *International Conference on Pattern Recognition*, pages A:117–120, Champaign, USA, June 1990.

[35] H. Samet. The quadtree and related hierarchical data structures. *ACM Computing Surveys*, 16(2):187–260, June 1984.

[36] D. Terzopoulos, A. Witkin, and M. Kass. Symmetry seeking models and object reconstruction. *Int. J. Computer Vision*, 1:211–221, 1987.

[37] V.S.Nalwa. Line-drawing interpretation: Bilateral symmetry. *IEEE Trans. on Pattern Analysis and Machine Intelligence*, 11(10):1117–1120, 1989.

[38] H. Weyl. *Symmetry*. Princeton Univ. Press, 1952.

[39] E. Yodogawa. Symmetropy, an entropy-like measure of visual symmetry. *Perception and Psychophysics*, 32(3):230–240, 1982.

[40] H. Zabrodsky and D. Avnir. Measuring symmetry in structural chemistry. In I. Hargittai, editor, *Advanced Molecular Structure Research*, volume 1. 1993.

[41] H. Zabrodsky and S. Peleg. Attentive transmission. *Journal of Visual Communication and Image Representation*, 1(2):189–198, November 1990.

[42] H. Zabrodsky, S. Peleg, and D. Avnir. Continuous symmetry measures, IV: Chirality. In Preparation.

[43] H. Zabrodsky, S. Peleg, and D. Avnir. Continuous symmetry measures II: Symmetry groups and the tetrahedron. *J. Am. Chem. Soc.*, 115 (to appear), 1993.

[44] H. Zabrodsky, S. Peleg, and D. Avnir. Continuous symmetry measures. *J. Am. Chem. Soc.*, 114:7843–7851, Sept 1992.